ELSEVIER

Biochimica et Biophysica Acta 1239 (1995) 122–132

BBA Biochimica et Biophysica Acta

Modelling packing interactions in parallel helix bundles: pentameric bundles of nicotinic receptor M2 helices

R. Sankararamakrishnan, M.S.P. Sansom *

Laboratory of Molecular Biophysics, University of Oxford, The Rex Richards Building, South Parks Road, Oxford, OX1 3QU, UK

Received 12 May 1995; accepted 4 July 1995

Abstract

The transbilayer pore of the nicotinic acetylcholine receptor (nAChR) is formed by a pentameric bundle of M2 helices. Models of pentameric bundles of M2 helices have been generated using simulated annealing via restrained molecular dynamics. The influence of: (a) the initial Cα template; and (b) screening of sidechain electrostatic interactions on the geometry of the resultant M2 helix bundles is explored. Parallel M2 helices, in the absence of sidechain electrostatic interactions, pack in accordance with simple ridges-in-grooves considerations. This results in a helix crossing angle of ca. +12°, corresponding to a left-handed coiled coil structure for the bundle as a whole. Tilting of M2 helices away from the central pore axis at their C-termini and/or inclusion of sidechain electrostatic interactions may perturb such ridges-in-grooves packing. In the most extreme cases right-handed coiled coils are formed. An interplay between inter-helix H-bonding and helix bundle geometry is revealed. The effects of changes in electrostatic screening on the dimensions of the pore mouth are described and the significance of these changes in the context of models for the nAChR pore domain is discussed.

Keywords: Ion channel; Nicotinic acetylcholine receptor; Transmembrane helix; Molecular dynamics; Electrostatics

1. Introduction

The nicotinic acetylcholine receptor (nAChR) is a cation-selective, ligand-gated ion channel, with subunit stoichiometry $\alpha_2\beta\gamma\delta$ [1]. The subunits are arranged quasi-symmetrically about a 5-fold axis, which coincides with the central trans-bilayer pore [2]. Chemical labelling experiments [3,4] and site-directed mutagenesis studies [5–7] suggest that the second putative transmembrane domain (M2) within the sequence of each subunit forms the lining of the channel [8–10]. Electron diffraction studies at 9 Å resolution reveal that five M2 helices, one from each subunit, form an approximately parallel bundle surrounding a central pore [11,12]. In the absence of atomic resolution structural data for nAChR, investigation of possible modes of packing of M2 helices within parallel bundles will facilitate modelling studies of the nAChR per se. Furthermore, the structural motif of a bundle of parallel transmembrane helices is of general importance, as it appears to occur in several ion channel proteins in addition to the nAChR [13–16]. Parallel helix bundles are also generated by a number of channel-forming peptides which self-assemble within lipid bilayers to form aqueous pores [17–20].

α-Helical coiled coils related to parallel helix bundles have been studied by several investigators both experimentally [21–23] and theoretically [24–27]. The packing of helices within such coiled coils may be compared with models for transmembrane (TM) helix bundles. In a previous study we modelled parallel bundles of simple hydrophobic and amphipathic helices [28]. These studies revealed a preference of simple hydrophobic TM helices (Ala_{20} and Leu_{20}) for left-handed coiled coils. However, the presence of polar side chains (Ser and Thr) within simple amphipathic helices appeared to perturb ridges-in-grooves helix packing. It is therefore of interest to investigate how electrostatic interactions of polar side chains within TM helices may alter the geometry of such helix bundles. As the M2 helices of nAChR contain several polar side chains (both charged and uncharged) they provide ideal candidates for such a study.

There is a long history of attempts to model the pore domain of the nAChR [4,14,29–31]. Such studies have employed a number of different methodologies in order to pack together the M2 helices. In this paper, we use simu-

* Corresponding author. Fax: +44 1865 510454. E-mail: mark@biop.ox.ac.uk.

SSDI 0005-2736(95)00165-4

lated annealing via restrained molecular dynamics (SA/MD) to model pentameric bundles of M2 helices. In this way we hope to automatically generate pore models consistent with a number of input assumptions and restraints, the latter derived by consideration of experimental (e.g. mutagenesis) data. The M2 sequence employed is that of chick $\alpha 7$ nAChR. This neuronal nAChR forms homopentameric channels (i.e. α_5) and has been the subject of extensive mutagenesis studies [9,10]. The SA/MD procedure employed generates an ensemble of structures which is amenable to statistical analysis. Several ensembles of M2 helix bundles have been generated, by varying factors such as: (a) the orientation of polar side chains relative to the centre of the pore; (b) the tilt angle of the M2 helices away from the central pore axis; and (c) the degree of screening of sidechain electrostatic interactions during MD simulations. The geometric and energetic properties of the resultant structures are analyzed in order to explore correlations between the extent of inter-helix electrostatic interactions and the deviation of M2 bundle geometry from that of an ideal left-handed coiled coil.

2. Methods

2.1. Computational

Molecular dynamics (MD) simulations and model building were carried out using XPLOR V3.1 [32] with the CHARMm PARAM19 parameter set [33]. Only those hydrogen atoms attached to the polar groups were represented explicitly; apolar groups were represented using extended atoms. Display and examination of bundles was carried out using QUANTA V4.0 (Molecular Simulations) and diagrams of the structures were drawn using MOLSCRIPT [34]. MD simulations were performed on DEC 3000 400 computers. All other calculations were carried out on Silicon Graphics R3000 workstations.

2.2. Simulated annealing via restrained molecular dynamics

Our implementation of the SA/MD method is similar to that of Nilges and Brünger [35], and has been used to model single TM helices [36–38], simple TM helix dimers [39] and simple TM helix bundles [28,40]. SA/MD is carried out in two stages. In *Stage 1* a slow annealing simulation is used to generate approximate coordinates for the polypeptide backbone and for the side chains, whilst the overall orientations of the helices remain fixed. In *Stage 2*, a restrained MD simulation, the helices are allowed to move and the sidechain and backbone conformations are refined.

The starting point for *Stage 1* of an SA/MD run is a Cα template corresponding to an ideal pentameric bundle. The remaining backbone and sidechain atoms of the TM helices are superimposed upon the Cα atoms of the corresponding residues. These atoms 'explode' from their Cα atoms, the positions of which remain fixed throughout *Stage 1*. Annealing starts at 1000 K, during which weights for covalent terms are gradually increased. A repulsive van der Waals term is slowly introduced after an initial delay. Once the scale factors of these components of the empirical energy function reach their final values, the system is cooled from 1000 to 300 K, in steps of 10 K and 0.5 ps. During the cooling, the van der Waals radii are reduced to 80% of their standard value to enable the atoms to pass by one another. Electrostatic terms are *not* included during *Stage 1*. Five structures are generated from a given Cα template.

Structures from *Stage 1* are each subjected to four restrained MD runs during *Stage 2*, resulting in an ensemble of $5 \times 4 = 20$ final structures. Initial velocities are assigned corresponding to 500 K. Harmonic restraints are imposed on Cα atoms at the beginning of *Stage 2* and are progressively relaxed as the temperature is reduced from 500 to 300 K. Inter- and intra-helix distance restraints are also introduced at this point (see below). On reaching 300 K, a 5 ps burst of constant temperature dynamics is performed, followed by 1000 steps of conjugate gradient energy minimization. During the latter burst of dynamics and energy minimization, no positional restraints are imposed on the Cα atoms, but inter- and intra-helix distance restraints are retained.

During *Stage 2* electrostatic interactions are introduced into the potential energy function. All main-chain atoms are assigned partial charges as defined by PARAM19 parameter set. Partial charges for sidechain atoms of *polar* residues are gradually scaled up, while the temperature is reduced from 500 to 300 K. In order to study the influence of electrostatic interactions involving polar side chains on helix packing a number of different electrostatic models have been employed (Table 1). These models differ in the degree of screening of electrostatic interactions between polar side chains. Such screening is controlled by: (a) varying the final scale factor applied to polar sidechain atoms; and (b) varying the dielectric model.

Table 1
Polar sidechain electrostatic models

Simulation	Scaling of charges [a]	Dielectric model
I	0.0	$\varepsilon = r$
II	$0.05 \rightarrow 0.4$	$\varepsilon = r$
III	$0.05 \rightarrow 1.0$	$\varepsilon = r$
IV	$0.05 \rightarrow 1.0$	$\varepsilon = 2$
V	$0.05 \rightarrow 1.0$	$\varepsilon = 1$

[a] Scaling of charges refers to the scale-factor applied to the partial atomic charges of polar side chains during *Stage 2* of SA/MD. To truncate distant interactions, models I, II and III employed a switch function from 5 Å to 9 Å, whereas models IV and V used a shift function with a 9 Å cutoff.

2.3. Distance restraints

Intra- and inter-helix distance restraints are imposed during *Stage 2*. Both classes of restraints are implemented using a biharmonic restraining function. Intra-helix restraints are used to maintain α-helical geometry and so act between the carbonyl O of residue i and the amide H of residue $(i+4)$. Target distance for these restrains are derived from α-helical H-bonding geometries observed in crystal structures of globular proteins [41].

Inter-helix restraints act between pairs of virtual atoms defined as the geometric centres of two groups of Cα atoms, one group within each of a pair of helices. The inter-helix restraints employed in the various simulations are defined in Table 2, and are discussed in more detail below. Note that in Table 2: (a) e.g. H_i(Cα:2–8) implies the geometric centre of Cα atoms of residues 2 to 8 of helix i; and (b) the pattern of restraints is cyclic, i.e. for a pentameric helix bundle, H_i to H_{i+1} implies restraints linking helix 1 to 2, 2 to 3, 3 to 4, 4 to 5 *and* 5 to 1.

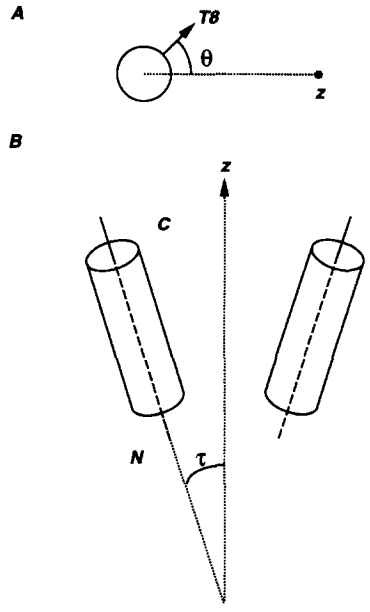

Fig. 1. Helix orientation parameters used to generate Cα templates. (A) illustrates the definition of θ; (B) the definition of τ. The 5-fold axis of the helix bundle is labelled z.

3. Results

3.1. M2 sequence and Cα templates

The starting point for generation of an ensemble of structures by SA/MD is a template which specifies the initial Cα coordinates of the helices. Several such Cα templates have been explored, taking into account experimental data on channel-lining side chains and on the approximate shape of the nAChR pore. Each template consisted of a pentameric bundle of chick α7 nAChR M2 helices, the sequence of which is:

Ac-E-K-I-**S**-L-G-I-**T**-V-L-L-**S**-L-**T**-V-F-M-L-L-V-A-E-NH_2
1′ 4′ 8′ 12′

The numbers below the sequence correspond to the channel-lining side chains shown in bold type and define the numbering scheme used throughout this paper, in which the glutamate residue of the cytoplasmic *intermediate ring* [10] of M2 is numbered 1′. The N-terminus of the helix is blocked with an acetyl group and the C-terminus with an amide group in order to mimic the effects of the preceding and following peptide bonds within the intact protein. The length of M2 and its position within the α7 nAChR sequence are consistent with current structural and mutagenesis data [10,11].

Cα templates were generated using idealized helix parameters (rise/residue = 1.5 Å; 3.6 residues/turn). The initial inter-axial separation of adjacent helices within a bundle was 9.4 Å, consistent with the results of crystallographic analyses of helix/helix packing in globular proteins [42]. Two parameters define the orientation of M2 helices within a Cα template: (a) θ, the angle of rotation of M2 about its major axis relative to the centre of the pore; and (b) τ, the tilt angle of M2 away from the central pore (z) axis (see Fig. 1).

Table 2
Target distances for inter-helix restraints

Restraint	Target distance (Å)		
	M2α7/τ0θ+20	M2α7/τ3θ+20	M2α7/τ6θ+20
	M2α7/τ0θ0	M2α7/τ3θ0	M2α7/τ6θ0
	M2α7/τ0θ−20	M2α7/τ3θ−20	M2α7/τ6θ−20
H_i(Cα:2–8) to H_{i+1}(Cα:2–8)	9.5	9.5	9.5
H_i(Cα:9–15) to H_{i+1}(Cα:9–15)	9.5	10.4	11.8
H_i(Cα:16–22) to H_{i+1}(Cα:16–22)	9.5	11.3	13.9
H_i(Cα:2–8) to H_{i+2}(Cα:2–8)	15.2	15.2	15.2
H_i(Cα:9–15) to H_{i+2}(Cα:9–15)	15.2	16.8	19.0
H_i(Cα:16–22) to H_{i+2}(Cα:16–22)	15.2	18.3	22.5

The hydrophilic face of M2, defined by residues 1′, 4′, 8′ and 12′, has been demonstrated to form the lining of the channel [5,10]. In particular, residues 8′ and 12′ have been implicated in interactions with a non-competitive blocker, QX-222, which binds within the lumen of the channel [6,7]. Thus, $\theta = 0°$ was defined to correspond to an M2 orientation in which Cα of T8′ pointed directly towards the pore (z) axis. Three values of θ were used in constructing Cα templates: $\theta = +20°$, 0° and $-20°$ (see Fig. 2). Thus, for $\theta = +20°$ the Cα atoms of residues T8′ and S12′, for $\theta = 0°$ Cα T8′ and for $\theta = -20°$ Cα S4′ and T8′ point towards the centre of the pore.

Three values of τ were considered: $\tau = 0°$ (i.e. M2 parallel to z), 3° and 6°. The latter two values correspond to tilting of the C-termini of the helices *away* from the pore axis, thus producing a wider mouth at the C-termini than at the N-termini. This is consistent with: (a) entry of bulky channel-blocking drugs, e.g. QX-222, into the lumen of the channel from the extracellular (i.e. C-terminal) side [7]; and (b) combined mutagenesis and electrophysiological studies which suggest that the narrowest region of the channel is closest to the N-termini of M2 [43]. The inter-helix distance restraints required to maintain these τ values during the simulations are given in Table 2.

Overall, nine different Cα templates were generated (three θ values and three τ values) using a grid search of Eulerian angles defining the helix orientations. The $\theta = 0°$ orientation was defined as that for which the sum of H_i(Cα:8′) to H_{i+1}(Cα:8′) distances across all helices of the bundle was at a minimum. Inter-helix distance restraints defining the τ values are given in Table 2.

3.2. Generation of ensembles

In generating ensembles of structures by SA/MD, the influence of electrostatic interactions between polar side chains on pore geometry was explored by employing different models for the screening of such interactions (Table 1). Model I omits sidechain electrostatic interactions entirely, providing a baseline against which the ef-

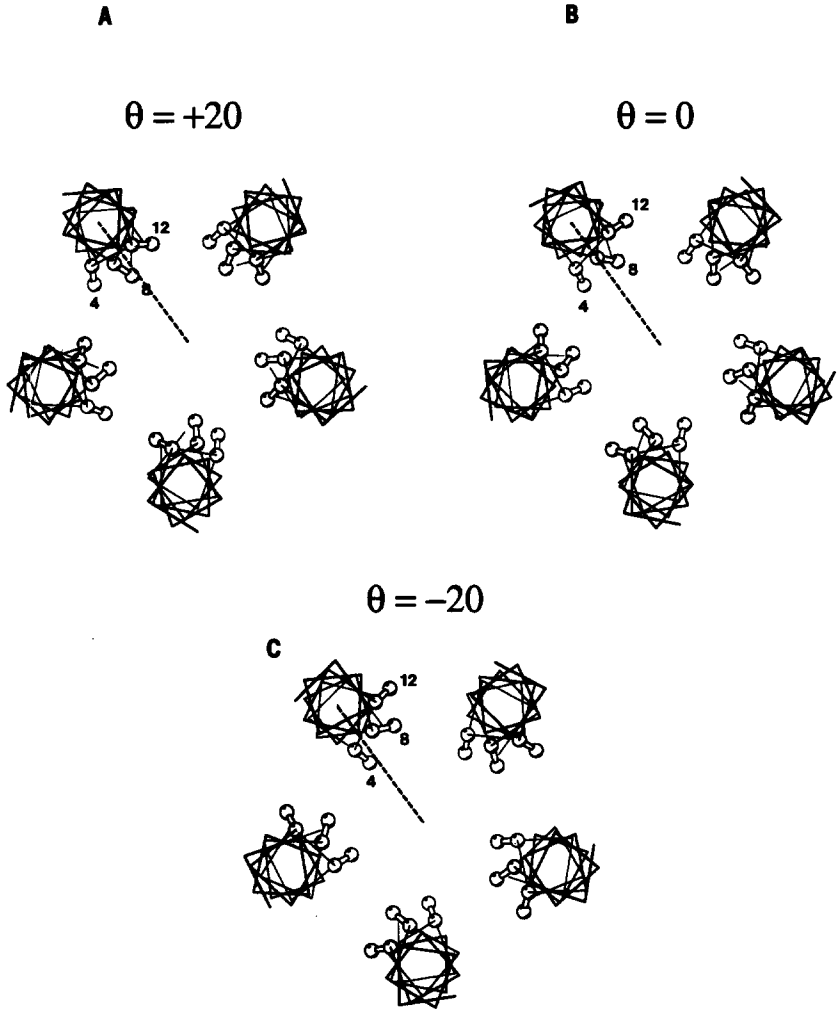

Fig. 2. Effect of the helix orientation angle θ on the positions of side chains S4′, T8′ and S12′ relative to the channel lumen. Selected structures are shown for $\theta = +20°$ (A; Cα template M2$\alpha 7/\tau 0\theta + 20$), 0° (B; M2$\alpha 7/\tau 0\theta 0$) and $-20°$ (C; M2$\alpha 7/\tau 0\theta - 20$). Note the numbering of the helices, which are shown with their C-termini towards the viewer.

fects of such interactions may be evaluated. In models II and III such interactions are screened (as in e.g. SA/MD studies of GCN4 helix dimers [35] and related coiled coils [44]), whereas in IV and V the sidechain electrostatic interactions are unscreened.

Together, nine Cα templates in combination with five electrostatic models were used to generate 45 distinct ensembles of M2 helix bundles, each containing 20 structures. In discussing the properties of these ensembles e.g. M2$\alpha 7/\tau 0\theta + 20$/IV will be used to refer to the ensemble generated from the $\tau = 0°$, $\theta = +20°$ Cα template, using sidechain electrostatic model IV. A typical ensemble (M2$\alpha 7/\tau 3\theta 0$/II) is shown in Fig. 3, illustrating the variation in bundle geometry which remains possible within a given set of restraints. In analyzing the ensembles thus generated, we will first consider patterns of inter-helix H-bonding interactions, and then relate these to geometric and energetic properties of the bundles.

3.3. Inter-helix H-bonds

Intra- and inter-helical interactions of polar side chains were identified by calculation of distances between potential interacting atom pairs, using a cut-off of 3.5 Å between non-H atoms. Three interactions were predominant within the ensembles: (a) an intra-helical ion pair between residues E1′ and K2′; (b) a H-bond from S4′ of helix i to E1′ of helix $(i-1)$; and (c) a H-bond between S4′ of helix i and K2′ of helix $(i-1)$. These interactions are designated as *EK*, *SE* and *SK*, respectively, and they are illustrated in Fig. 4. Their frequencies of occurrence in the different ensembles are provided in Table 3.

First consider the *intra*-helical interaction, *EK*. As in previous SA/MD studies of isolated M2 helices [38] the main influence on the frequency of this interaction is the degree of screening of electrostatic interactions. Model I, which excludes sidechain electrostatic interactions, indicates that close approach of E1′ and K2′ on the basis of purely steric criteria occurs relatively infrequently. As the degree of electrostatic screening is reduced (from II to V) the frequency of *EK* interactions increases, until in V such ion pairs are found in almost all helices of the nine ensembles. With intermediate degrees of screening, there is some dependency of EK pair formation on the Cα template geometry (e.g. M2$\alpha 7/\tau 3\theta - 20$/II vs. M2$\alpha 7/\tau 3\theta + 20$/II), which may in turn reflect changes in the frequency of competing inter-helix interactions involving the E1′ and K2′ side chains.

Turning to *inter*-helical interactions, the situation is more complex, with an interplay between the initial Cα template and the electrostatic model in determining the final structure. For $\theta = +20°$, S4′ is positioned at the helix-i/helix-$(i-1)$ interface (see Fig. 2). As θ is reduced, S4′ is rotated away from the interface towards the lumen of the pore. At the same time residue S12′ is moved away from the lumen, towards the helix-i/helix-$(i+1)$ interface. This rotation alters the frequency of *inter*-helix H-bonds formed by S4′. In general, the frequency of *SE* and *SK* H-bonds falls as θ is decreased and S4′ is moved away from the interfacial region. Furthermore, for $\theta = 0°$, the frequency of *SE* and *SK* interactions increases as τ is increased. Both of these trends are most evident for electrostatic models III and IV, which perhaps may be considered as approximations to the degree of screening expected within a transbilayer helix bundle.

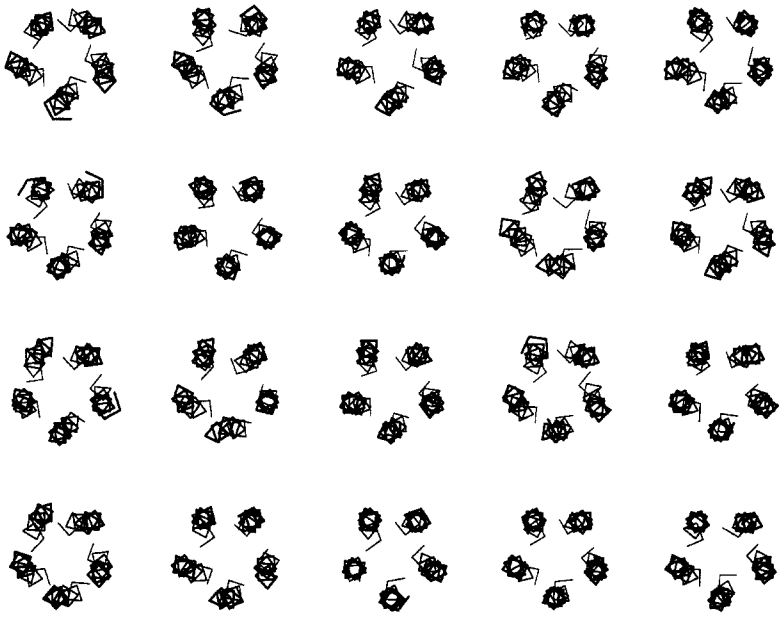

Fig. 3. Example of an ensemble of structures (M2$\alpha 7/\tau 3\theta 0$/II) shown as Cα traces with their C-termini towards the viewer. In the array of structures, the four rows correspond to the four *Stage 1* runs, and five columns to the subsequent five *Stage 2* runs used to generate the final ensemble of twenty structures (see Methods for details).

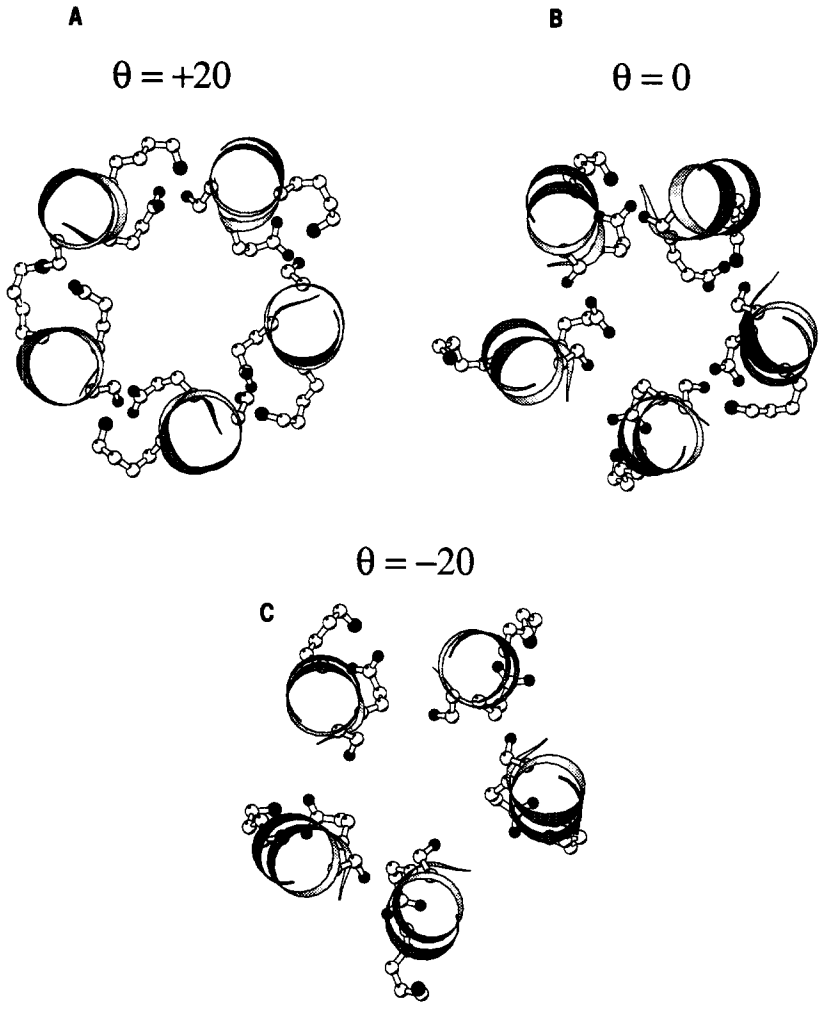

Fig. 4. Inter-helix H-bonding patterns. The first two turns of the helix and the side chains of residues E1′, K2′ and S4′ are shown for structures from ensembles (A) M2$\alpha 7/\tau 3\theta + 20$/III, (B) M2$\alpha 7/\tau 3\theta 0$/III, and (C) M2$\alpha 7/\tau 3\theta - 20$/III. For simplicity, H atoms are omitted from the side chains.

Overall, this analysis reveals that statistical patterns of H-bond formation within M2 helix bundles depend upon both the initial orientations of the helices in the Cα templates, and on the strength of sidechain electrostatic interactions. Previous studies on simple amphipathic helix bundles suggested that inter-helix H-bond formation may

Table 3
Intra- and inter-helical interactions of polar side chains [a]

Cα template	Model I			Model II			Model III			Model IV			Model V		
	EK	*SE*	*SK*	*EK*	*SE*	*SK*	*EK*	*SE*	*SK*	*EK*	*SE*	*SK*	*EK*	*SE*	*SK*
M2$\alpha 7/\tau 0\theta + 20$	3	14	13	27	40	35	93	87	78	100	75	67	100	90	88
M2$\alpha 7/\tau 3\theta + 20$	10	15	16	34	32	35	98	83	81	100	88	78	100	98	99
M2$\alpha 7/\tau 6\theta + 20$	3	31	21	30	51	31	94	90	78	98	80	63	100	96	93
M2$\alpha 7/\tau 0\theta 0$	4	55	1	34	48	1	81	39	9	89	34	6	92	42	25
M2$\alpha 7/\tau 3\theta 0$	4	41	0	28	44	2	80	50	27	89	36	10	88	60	37
M2$\alpha 7/\tau 6\theta 0$	0	45	2	29	37	7	88	49	29	87	47	21	95	62	43
M2$\alpha 7/\tau 0\theta - 20$	9	40	0	55	33	0	93	21	1	97	15	0	100	20	6
M2$\alpha 7/\tau 3\theta - 20$	13	30	0	57	11	0	92	9	0	95	13	1	98	11	3
M2$\alpha 7/\tau 6\theta - 20$	9	17	0	54	11	1	92	10	3	95	7	2	97	6	4

[a] The tabulated numbers are the frequencies of interactions *EK*, *SE* and *SK* in the ensembles. *EK* is an intra-helical E1′ to K2′ ion pair. *SE* and *SK* are inter-helical H-bonds between S4′ of the ith helix and E1′ of the $(i-1)$th helix (*SE*), and between S4′ of the ith helix and K2′ of the $(i-1)$th helix (*SK*).

Table 4
Crossing angles (Ω) for adjacent helices in bundles [a]

Model	M2α7/τ0θ+20	M2α7/τ3θ+20	M2α7/τ6θ+20
I	+10.3 (±3.8)	+12.8 (±3.5)	+0.9 (±8.6)
II	+7.9 (±2.2)	+11.5 (±2.9)	−3.9 (±8.8)
III	+4.8 (±2.2)	+8.5 (±2.9)	−9.6 (±7.4)
IV	+3.6 (±2.3)	+10.3 (±1.9)	−5.2 (±8.1)
V	−0.8 (±2.6)	+7.8 (±2.4)	−15.5 (±3.3)
Model	M2α7/τ0θ0	M2α7/τ3θ0	M2α7/τ6θ0
I	+11.9 (±1.6)	+8.3 (±2.3)	+6.6 (±8.5)
II	+11.1 (±1.3)	+8.9 (±2.6)	+5.6 (±7.1)
III	+10.2 (±2.1)	+4.7 (±3.4)	+6.9 (±6.5)
IV	+10.3 (±2.7)	+5.3 (±3.7)	+5.5 (±8.3)
V	+8.5 (±1.8)	+1.9 (±3.7)	+1.8 (±8.2)
Model	M2α7/τ0θ−20	M2α7/τ3θ−20	M2α7/τ6θ−20
I	+14.9 (±1.6)	+5.9 (±6.0)	+2.8 (±8.2)
II	+14.2 (±1.5)	+4.9 (±6.3)	+6.6 (±7.7)
III	+13.0 (±2.3)	+6.2 (±7.1)	−0.2 (±7.7)
IV	+13.7 (±2.3)	+5.2 (±5.5)	+0.4 (±7.2)
V	+13.8 (±1.9)	+6.1 (±6.5)	+1.5 (±7.3)

[a] Crossing angles (in degrees) are given as the mean (± standard deviation) for all adjacent helix pairs within an ensemble.

perturb packing of helices away from that anticipated on the basis of ridges-in-grooves considerations [28]. The variation in patterns of H-bonding between M2α7 ensembles enables this effect to be analyzed in greater detail.

3.4. Geometric properties

The crossing angle (Ω) between adjacent helices may be used to describe the geometry of packing of helices within a bundle. In particular, this indicates the handedness of a coiled coil, with a positive Ω corresponding to a left-handed coiled coil. Helix crossing angles were determined for each helix pair as described by Chothia et al. [42], and ensemble averages of Ω were determined across all adjacent helix pairs within an ensemble, as summarized in Table 4.

The results of this analysis reveal an interdependence of the geometry of helix packing and of the pattern of inter-helical H-bonding. Consider first the parallel ($\tau = 0°$) helix bundles. For $\theta = -20°$ and 0° in the absence of strong sidechain electrostatic interactions (models I and II) these ensembles exhibit approximate class 3–4 ridges-in-grooves helix packing (for which $\langle \Omega \rangle = +10$ to $+20°$), as is seen in pentameric bundles of simple hydrophobic helices [28]. However, if $\theta = +20°$, the presence of strong inter-helix electrostatic interactions (in III to V) perturbs such packing towards lower Ω (less supercoiled) values. The extent of such perturbation correlates well with the frequency of *SE* and *SK* inter-helical H-bonds in these ensembles. Thus, with parallel M2 helices, the presence of S4′ at the helix/helix interface can perturb simple ridges-in-grooves packing.

Now consider the effects of increasing the helix tilt angle τ. For $\theta = 0°$ and $-20°$ the main effect of increasing τ is to weaken the ridges-in-grooves packing observed for the $\tau = 0°$ template. This is evident from the increased standard deviation of Ω, indicating a greater heterogeneity of helix packing within these ensembles. For $\theta = +20°$, both τ and the strength of sidechain electrostatic interactions influence helix packing. In the most extreme comparison, between M2α7/τ0θ+20/I and M2α7/τ6θ+20/V, this results is a switch from a left-handed ($\langle \Omega \rangle = +10°$) to a right-handed coiled coil ($\langle \Omega \rangle = -16°$), Fig. 5. This correlates with nearly 100% formation of inter-helix *SE* and *SK* H-bonds in the latter ensemble, compared to no such interactions in the former. Furthermore, the change in τ from 0° to 6° results in loss of ridges-in-grooves

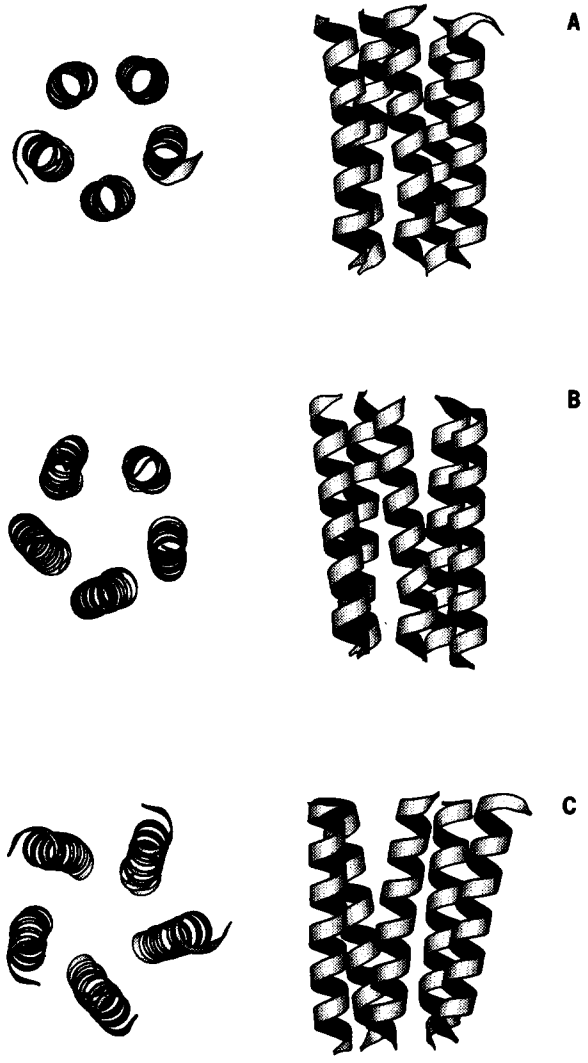

Fig. 5. Effect of Cα template parameters (τ,θ) and of the sidechain electrostatic model on the final bundle geometry. Helix ribbon diagrams of bundles are shown for selected structures from ensembles (A) M2α7/τ0θ+20/III, (B) M2α7/τ3θ+20/III and (C) M2α7/τ6θ+20/III, for which the mean Ω values are +4.8°, +8.5° and −9.6°, respectively. For each ensemble, the left-hand diagram is a view down z, with the C-termini towards the viewer, whereas the right-hand view has the C-termini of the helices uppermost.

Table 5
Helix–helix van der Waals interaction energies (ΔE_{VDW}) [a]

Model	M2α7/τ0θ+20	M2α7/τ3θ+20	M2α7/τ6θ+20
I	−245.8 (±9.1)	−202.1 (±8.8)	−146.9 (±7.7)
II	−220.2 (±9.2)	−177.4 (±8.2)	−133.8 (±6.5)
III	−174.5 (±7.6)	−143.9 (±5.6)	−100.6 (±8.2)
IV	−191.1 (±5.5)	−164.8 (±4.5)	−119.3 (±7.2)
V	−173.4 (±7.1)	−146.1 (±5.2)	−100.0 (±7.3)
Model	M2α7/τ0θ0	M2α7/τ3θ0	M2α7/τ6θ0
I	−232.0 (±8.6)	−186.8 (±7.9)	−127.2 (±6.6)
II	−205.7 (±9.3)	−173.9 (±8.5)	−117.7 (±10.3)
III	−180.7 (±5.9)	−148.4 (±7.0)	−95.3 (±7.1)
IV	−190.6 (±6.4)	−150.4 (±6.4)	−106.3 (±6.2)
V	−172.9 (±7.2)	−139.9 (±7.0)	−98.5 (±4.9)
Model	M2α7/τ0θ−20	M2α7/τ3θ−20	M2α7/τ6θ−20
I	−231.4 (±11.9)	−173.9 (±14.1)	−111.2 (±11.3)
II	−209.3 (±8.4)	−157.1 (±9.9)	−103.5 (±6.2)
III	−189.3 (±7.4)	−149.1 (±8.4)	−96.8 (±7.7)
IV	−190.8 (±6.3)	−149.7 (±8.5)	−98.9 (±4.5)
V	−182.7 (±7.2)	−143.3 (±9.3)	−97.2 (±7.5)

[a] The mean (± standard deviation) of ΔE_{VDW} (kcal/mol) is given for each ensemble.

interactions of the predominantly hydrophobic side chains present in the C-terminal half of M2.

3.5. Helix–helix interaction energies

It is informative to relate the strength of interactions between helices of M2 bundles to the geometrical properties of such bundles. Helix–helix interaction energies were calculated as

$$\Delta E = E_{BUNDLE} - \sum_i E_i$$

where E_{BUNDLE} is the potential energy of the intact bundle and E_i is the potential energy of constituent helix i in isolation, and where summation is over all the five helices of the bundle. Both the van der Waals (ΔE_{VDW}) and electrostatic components (ΔE_{ELEC}) of interaction energies were evaluated and the results are presented in Tables 5 and 6, respectively.

Van der Waals energies provide a measure of the extent of simple packing interactions between helices. Two trends are evident (Table 5): (a) a decrease in the magnitude of ΔE_{VDW} as the strength of electrostatic interactions increases (i.e. I to V); and (b) a decrease in the magnitude of ΔE_{VDW} as τ is increased. The first trend reflects competition between electrostatic and van der Waals interactions; the latter trend a weakening of van der Waals interactions as tilting reduces the contact areas of the helices. This analysis confirms the proposal that the extent of perturbation of class 3–4 ridges-in-grooves packing (i.e. left-handed supercoiling) correlates with weakening of van der Waals interactions at the expense of electrostatic interactions. This is evident by comparison of the interaction energies of e.g. ensembles M2α7/τ0θ+20/I and M2α7/τ6θ+20/V. In this example the *total* interaction energies are approximately equal (ca. −240 kcal/mol) but a shift from E_{VDW} = −246 kcal/mol (M2α7/τ0θ+20/I) to E_{VDW} = −100 kcal/mol (M2α7/τ6θ+20/V) is correlated with a switch in $\langle\Omega\rangle$ from +10° to −16°.

3.6. Pore radius profiles

The radius of the pore through the M2 helix bundles was determined using HOLE [28,45]. Average pore radius profiles were calculated for each ensemble, and are shown in Fig. 6 for models M2α7/τ0θ0 and M2α7/τ6θ0. As anticipated, the pore radius at the C-terminal mouth of the bundle increased as τ was increased from 0° to 6°. The influence of electrostatic interactions on the pore radius profiles at the N-terminal mouth, where EK pairs are located, is evident by comparison of models I, II and III (in all cases the profiles for models IV and V are similar to those for model III). The pore radius at the N-terminal mouth is directly related to the presence or absence of salt-bridges between E1′ and K2′ side chains. Previous studies [38] on isolated M2 helices revealed that the extent of EK interactions was strongly influenced by the treatment of electrostatic interactions. In model I, which excludes sidechain electrostatic interactions, the frequency of EK interactions is negligible. As a result, the glutamate side chains point towards the centre of the pore reducing its radius close to the point of occlusion. In contrast, in model III, IV and V, for which electrostatic interactions are pronounced, EK salt-bridges are found in almost all

Table 6
Helix–helix electrostatic interaction energies (ΔE_{ELEC}) [a]

Model	M2α7/τ0θ+20	M2α7/τ3θ+20	M2α7/τ6θ+20
I	+1.7 (±1.5)	+1.3 (±1.4))	+0.7 (±3.9)
II	−0.9 (±27.5)	−5.9 (±4.5)	−7.6 (±3.7)
III	−116.1 (±22.9)	−125.8 (±21.9)	−122.1 (±24.4)
IV	−41.7 (±11.2)	−43.9 (±8.8)	−47.6 (±24.6)
V	−129.7 (±19.1)	−140.9 (±6.6)	−131.2 (±8.5)
Model	M2α7/τ0θ0	M2α7/τ3θ0	M2α7/τ6θ0
I	−1.2 (±2.0)	+0.8 (±1.4)	+1.8 (±0.6)
II	−4.7 (±3.9)	−5.5 (±4.3)	−9.7 (±4.1)
III	−50.6 (±26.4)	−70.9 (±35.2)	−59.8 (±22.7)
IV	−17.3 (±10.6)	−19.4 (±14.7)	−28.6 (±9.4)
V	−70.9 (±22.1)	−93.3 (±34.5)	−88.8 (±18.8)
Model	M2α7/τ0θ−20	M2α7/τ3θ−20	M2α7/τ6θ−20
I	−1.3 (±1.9)	+0.8 (±1.8)	+1.7 (±1.4)
II	−0.3 (±3.9)	+0.6 (±2.6)	−4.1 (±2.3)
III	−29.9 (±10.8)	−17.9 (±10.3)	−27.5 (±22.3)
IV	−19.7 (±15.1)	−14.3 (±9.1)	−14.9 (±8.0)
V	−44.1 (±22.1)	−33.8 (±15.8)	−42.9 (±17.3)

[a] The mean (± standard deviation) of ΔE_{ELEC} (kcal/mol) is given for each ensemble. Note that in all cases ΔE_{ELEC} is calculated using the electrostatic models and final scaling of partial charges defined in Table 1.

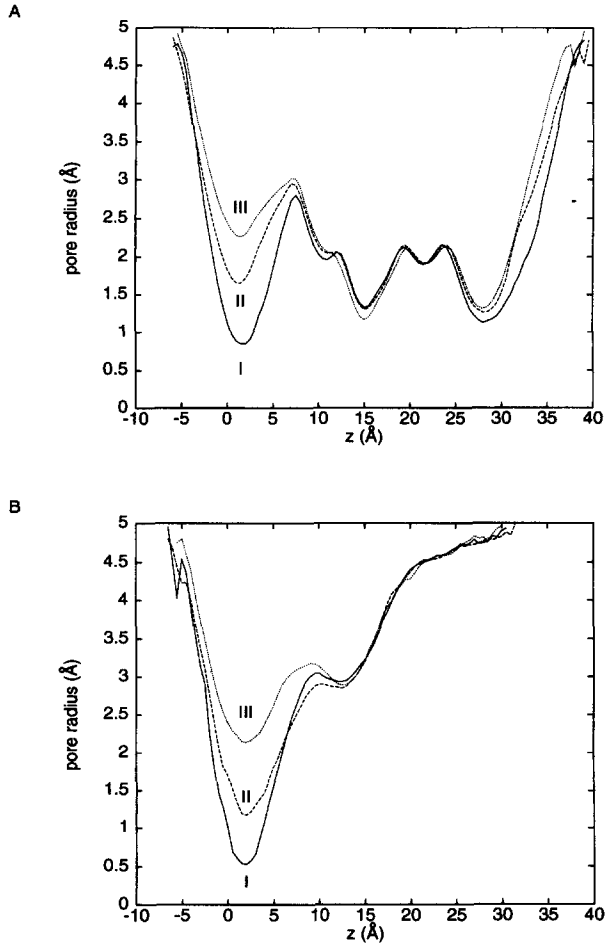

Fig. 6. Pore radius profile for ensembles M2$\alpha 7/\tau 0\theta 0$ (A) and M2$\alpha 7/\tau 6\theta 0$ (B). Profiles shown are averages across each ensemble. Profiles corresponding to electrostatic models I, II and III are shown as solid, broken and dotted lines, respectively. The N-terminal mouth of the pore is at $z \approx 0$ Å and the C-terminal mouth at $z \approx +30$ Å.

helices of all ensembles irrespective of the starting template. When such interactions are present, the side chain of E1′ curls back away from the lumen of the pore to form a salt-bridge with the K2′ side chain. This results in widening of the pore at the N-terminal mouth. Model II, which has an intermediate level of EK interactions exhibits an intermediate pore radius (Fig. 6). Thus it is clear that altering the treatment of electrostatic interactions can have a significant effect on the pore dimensions.

The conformations of EK pairs are of especially importance, since within intact nAChR, E1′ residues form a functionally important 'intermediate ring' of side chains which is believed to constitute a narrow entrance to the channel. In intact nAChR, EK pairs are thought to lie in the mouth of the channel, close to membrane/water interface. The dielectric constant ε in the interface region may be expected to be somewhere between 2 and 80 [46]. Thus degree of screening of electrostatic interactions (as in model III) would occur in this region. However, it is difficult to estimate the extent of such screening. Furthermore, changes in the local electrostatic field due to permeant cations may generate conformational transitions in E1′ side chains, thus perturbing the pore radius.

4. Discussion

4.1. Cα templates

It is important to be clear about the role of the Cα template in SA/MD modelling of channels formed by parallel TM helix bundles. The Cα template is constructed to represent available experimental (e.g. mutagenesis) data. SA/MD is then used to automatically generate models consistent with this data. However, in the process of generating such models, structural features not explicit in the Cα template emerge. For example, in all of the Cα templates employed in the current study the initial helix crossing angle is $\Omega = 0°$, yet in the final ensembles coiled coils are present. Thus, the SA/MD generated structures both satisfy experimentally derived restraints, and populate a (local) potential energy minimum.

Values for the two parameters used to construct the Cα templates were estimated on the basis of two categories of experimental data. Mutagenesis and chemical labelling data identify those side chains of M2 which line the lumen of the channel [8–10] thus allowing θ to be specified quite precisely. From such data it is evident that side chains 4′, 8′ and 12′ point towards the channel lumen. Non-competitive blockers of nAChR, e.g. QX-222, have been demonstrated to interact with side chains in the central region of M2 [6,7]. To enable access of QX-222 to this region suggests that a degree of helix tilt (τ) is required in order to widen the C-terminal mouth of the pore. Such tilting of the M2 helices has been explored in a number of other modelling studies of the nAChR pore [4,30]

4.2. Electrostatic models

Exactly how to model electrostatic interactions within a transbilayer pore raises some problems. Thus, the helix bundle is surrounded by a region of dielectric ca. $\varepsilon = 4$. The mouths of the pore are exposed to bulk aqueous solvent ($\varepsilon = 80$) whilst inside the pore the effective dielectric will be somewhat lower [47,48] as a result of partial immobilization of water molecules. One solution to this problem might be to explicitly include bilayer, solvent and counterions in the MD simulations. However, this would be computationally expensive and difficult to implement in the absence of structural data for the remainder of the nAChR protein. In an attempt to clarify the role of electrostatic interactions we have adopted an alternative approach in which we vary the degree of electrostatic screening. Utilization of this approach to study isolated M2 helices revealed that changes in the degree of screening produced marked changes in intra-helical interactions of polar side chains [38].

In this context it is interesting to note that in their simulations of GCN4 and of related coiled coil structures Brünger and colleagues [35,44] scaled polar sidechain partial charges (by 0.3) and used distance dependent screening of electrostatic interactions. In studies of glycophorin TM helix dimers, for which a right-handed supercoil was proposed, electrostatic interactions were unscreened [49]. In view of our results concerning the effects of treatment of sidechain electrostatic interactions on bundle geometry, it might be interesting to perform similar analyses for these structurally related systems.

4.3. Implications of results

What are the implications of our simulation results for models of the nAChR transbilayer pore? The clearest conclusion is that the interplay between the Cα template and the electrostatic model complicates modelling of M2 helix bundle geometry. In this context it is valuable to compare the present results with the recent cryo-electron microscopy (EM) studies of the open [12] and closed [11] conformations of the nAChR. In the open state, the pore is formed by a bundle of α-helices which has a pronounced right-handed twist, whereas in the closed state, the helices twist around each other in a left-handed fashion. A change in sidechain–sidechain interactions between adjacent M2 helices is proposed to occur when the transition between open and closed states is made. Although the proposed changes in interactions involve mainly hydrophobic residues, changes in interactions involving polar residues cannot be ruled out. Examination of average crossing angles (Table 4) revealed that the template M2$\alpha 7/\tau 6\theta +$ 20 resulted in a negative crossing angle (i.e. right-handed coiled-coil of helices) when sidechain electrostatic interactions were included (electrostatic models II to V). In a subsequent study [50] we demonstrate that this model permits passage of large permeant cations (e.g. trimethylamine [51]), as well as preventing permeation by non-competitive blockers (e.g. QX-222) as observed in experimental studies [7].

It should be mentioned that the helices observed in the EM studies of both the open and closed states are kinked. MD studies on isolated M2 helices did not identify a unique kinked structure [37]. It has been suggested that the kink in M2 may be produced by small, cumulative distortions of the polypeptide backbone from an ideal α-helical geometry [52]. The widening of the pore at the extracellular mouth is in part due to the kink in the helices. The EM studies reveal that in the open state the pore narrows fairly uniformly from the outer to the inner face of the membrane [12]. Though we have not introduced any kink into the constituent helices of bundles, those models with $\tau = 3°$ or 6° exhibit such a uniform narrowing of the pore. Thus such models provide an approximate representation of the open state of the nAChR.

A second implication of the simulation studies is that if 'channel-lining' side chains such as S4′ participate in helix–helix interactions (e.g. at frequencies of ca. 80% for *SE* and *SK* in M2$\alpha 7/\tau 3\theta + 20$/III, see Table 3) then mutations of such side chains may not only alter the nature of the channel lining, but may perturb the overall pore geometry. This may complicate the interpretation of mutagenesis data and suggests that detailed modelling studies will be required to establish the extent to which various side chains fulfil a purely channel-lining role.

Our results also have implications with respect to modelling studies of other ion channels. For example, it has been suggested that inter-helix H-bonds are important in stabilization of channels formed by bundles of the 20 residue peptaibol alamethicin [19,53]. Molecular modelling studies using SA/MD can reveal the influence of such H-bonds on the geometry of alamethicin helix bundles and thus on the properties of the channels [39].

4.4. Overall conclusions

Studies on pentameric M2 bundles show that SA/MD may be used to analyze the influence of electrostatic interactions on TM helix bundle geometry. In particular, by varying the Cα template and the electrostatic model it is possible to switch between a left-handed and a right-handed coiled coil. Thus, in order to obtain a working model for the structure of the nAChR pore, it will be necessary to 'screen' SA/MD generated structures with respect to their predicted interactions with permeant and with impermeant cations [54,55]. It will also be necessary to incorporate restraints derived from the low resolution EM structural data into our simulations [52]. The results of such calculations will form the subject of a future communication.

Acknowledgements

This work was supported by a grant from the Wellcome Trust. Our thanks to the Oxford Centre for Molecular Sciences for access to computational facilities, and to our colleagues Dr. Ian Kerr, Mr. Jason Breed, Mr. Hyeon Son and Mr. Phil Biggin for their interest in this work. Thanks to Dr. Oliver Smart for his program HOLE.

References

[1] Stroud, R.M., McCarthy, M.P. and Shuster, M. (1990) Biochemistry 50, 1107–11023.
[2] Unwin, N. (1989) Neuron 3, 665–676.
[3] Giraudat, J., Dennis, M., Heidmann, T., Haumont, P.Y., Lederer, F. and Changeux, J.P. (1987) Biochemistry 26, 2410–2418.
[4] Hucho, F., Oberthür, W. and Lottspeich, F. (1986) FEBS Lett. 205, 137–142.
[5] Imoto, K., Busch, C., Sakmann, B., Mishina, M., Konno, T., Nakai, J., Buyo, H., Mori, Y., Kukuda, K. and Numa, S. (1988) Nature 335, 645–648.

[6] Leonard, R.J., Labarca, C.G., Charnet, P., Davidson, N. and Lester, H.A. (1988) Science 242, 1578–1581.
[7] Charnet, P., Labarca, C., Leonard, R.J., Vogelaar, N.J., Czyzyk, L., Gouin, A., Davidson, N. and Lester, H.A. (1990) Neuron 2, 87–95.
[8] Lester, H. (1992) Annu. Rev. Biophys. Biomol. Struct. 21, 267–292.
[9] Changeux, J.P., Galzi, J.I., Devillers-Thiéry, A. and Bertrand, D. (1992) Quart. Rev. Biophys. 25, 395–432.
[10] Bertrand, D., Galzi, J.L., Devillers-Thiéry, A., Bertrand, S. and Changeux, J.P. (1993) Curr. Opin. Cell Biol. 5, 688–693.
[11] Unwin, N. (1993) J. Mol. Biol. 229, 1101–1124.
[12] Unwin, N. (1995) Nature 373, 37–43.
[13] Oiki, S., Madison, V. and Montal, M. (1990) Proteins Struct. Func. Genet. 8, 226–236.
[14] Montal, M.O., Iwamoto, T., Tomich, J.M. and Montal, M. (1993) FEBS Lett. 320, 261–266.
[15] Sansom, M.S.P. and Kerr, I.D. (1993) Protein Eng. 6, 65–74.
[16] Arkin, I.T., Adams, P.D., MacKenzie, K.R., Lemmon, M.A., Brünger, A.T. and Engelman, D.M. (1994) EMBO J. 13, 4757–4764.
[17] Sansom, M.S.P. (1991) Prog. Biophys. Mol. Biol. 55, 139–236.
[18] Sansom, M.S.P. (1993) Eur. Biophys. J. 22, 105–124.
[19] Sansom, M.S.P. (1993) Quart. Rev. Biophys. 26, 365–421.
[20] Kerr, I.D., Dufourcq, J., Rice, J.A., Fredkin, D.R. and Sansom, M.S.P. (1995) Biochim. Biophys. Acta 1236, 219–227.
[21] O'Shea, E.K., Klemm, J.D., Kim, P.S. and Alber, T. (1991) Science 254, 539–544.
[22] Harbury, P.B., Zhang, T., Kim, P.S. and Alber, T. (1993) Science 262, 1401–1407.
[23] Lovejoy, B., Choe, S., Cascio, D., McRorie, D.K., DeGrado, W.F. and Eisenberg, D. (1993) Science 259, 1288–1293.
[24] Adamson, J.G., Zhou, N.E. and Hodges, R.S. (1993) Curr. Opin. Biotechnol. 4, 428–437.
[25] Seo, J. and Cohen, C. (1993) Proteins Struct. Func. Genet. 15, 223–234.
[26] Zhang, L. and Hermans, J. (1993) Proteins Struct. Func. Genet. 16, 384–392.
[27] Cohen, C. and Parry, D.A.D. (1994) Science 263, 488–489.
[28] Kerr, I.D., Sankararamakrishnan, R., Smart, O.S. and Sansom, M.S.P. (1994) Biophys. J. 67, 1501–1515.
[29] Guy, H.R. and Hucho, F. (1987) Trends Neurosci. 10, 318–321.
[30] Furois-Corbin, S. and Pullman, A. (1989) Biochim. Biophys. Acta 984, 339–350.
[31] Ortells, M.O. and Lunt, G.G. (1994) Receptors Channels 2, 53–59.
[32] Brünger, A.T. (1992) X-plor Version 3.1, Yale University Press, New Haven, CT.
[33] Brooks, B.R., Bruccoleri, R.E., Olafson, B.D., States, D.J., Swaminathan, S. and Karplus, M. (1983) J. Comp. Chem. 4, 187–217.
[34] Kraulis, P.J. (1991) J. Appl. Cryst. 24, 946–950.
[35] Nilges, M. and Brünger, A.T. (1991) Protein Eng. 4, 649–659.
[36] Kerr, I.D. and Sansom, M.S.P. (1993) Eur. Biophys. J. 22, 269–277.
[37] Sankararamakrishnan, R. and Sansom, M.S.P. (1994) Biopolymers 34, 1647–1657.
[38] Sankararamakrishnan, R. and Sansom, M.S.P. (1995) Biophys. Chem. 55, 215–230.
[39] Breed, J., Kerr, I.D., Sankararamakrishnan, R. and Sansom, M.S.P. (1995) Biopolymers 35, 639–655.
[40] Sansom, M.S.P., Son, H.S., Sankararamakrishnan, R., Kerr, I.D. and Breed, J. (1995) Biophys. J. 68, 1295–1310.
[41] Baker, E.N. and Hubbard, R.E. (1984) Prog. Biophys. Mol. Biol. 44, 97–179.
[42] Chothia, C., Levitt, M. and Richardson, D. (1981) J. Mol. Biol. 145, 215–250.
[43] Villarroel, A., Herlitze, S., Koenen, M. and Sakmann, B. (1991) Proc. R. Soc. Lond. B 243, 69–74.
[44] DeLano, W.L. and Brünger, A.T. (1994) Proteins Struct. Func. Genet. 20, 105–123.
[45] Smart, O.S., Goodfellow, J.M. and Wallace, B.A. (1993) Biophys. J. 65, 2455–2460.
[46] Karshikoff, A., Spassov, V., Cowan, S.W., Ladenstein, R. and Schirmer, T. (1994) J. Mol. Biol. 240, 372–384.
[47] Partenskii, M.B. and Jordan, P.C. (1992) J. Phys. Chem. 96, 3906–3910.
[48] Partenskii, M.B., Dorman, V. and Jordan, P.C. (1994) Biophys. J. 67, 1429–1438.
[49] Treutlein, H.R., Lemmon, M.A., Engelman, D.M. and Brünger, A.T. (1992) Biochem. 31, 12726–12733.
[50] Sankararamakrishnan, R. and Sansom, M.S.P. (1995) Biophys. J. 68, A378.
[51] Dwyer, T.M., Adams, D.J. and Hille, B. (1980) J. Gen. Physiol. 75, 469–492.
[52] Sansom, M.S.P., Sankararamakrishnan, R. and Kerr, I.D. (1995) Nature Struct. Biol. 2, 624–631.
[53] Fox, R.O. and Richards, F.M. (1982) Nature 300, 325–330.
[54] Sankararamakrishnan, R. and Sansom, M.S.P. (1995) in Membrane Protein Models: Experiment, Theory and Speculation (Findlay, J., ed.).
[55] Sankararamakrishnan, R. and Sansom, M.S.P. (1995) (in preparation).